# ON THE FLIGHT PERFORMANCE IMPACT OF LANDING GEAR DRAG REDUCTION METHODS FOR UNMANNED AIR VEHICLES

F. Götten, F. Finger, M. Havermann, C. Braun
Department of Aerospace Engineering, FH Aachen University of Applied Sciences, Aachen, Germany

F. Gómez, C. Bil
School of Engineering, RMIT University, Melbourne, Australia

**Abstract**

The flight performance impact of three different landing gear configurations on a small, fixed-wing UAV is analyzed with a combination of RANS CFD calculations and an incremental flight performance algorithm. A standard fixed landing gear configuration is taken as a baseline, while the influence of retracting the landing gear or applying streamlined fairings is investigated. A retraction leads to a significant parasite drag reduction, while also fairings promise large savings. The increase in lift-to-drag ratio is reduced at high lift coefficients due to the influence of induced drag. All configurations are tested on three different design missions with an incremental flight performance algorithm. A trade-off study is performed using the retracted or faired landing gear's weight increase as a variable. The analysis reveals only small mission performance gains as the aerodynamic improvements are negated by weight penalties. A new workflow for decision-making is presented that allows to estimate if a change in landing gear configuration is beneficial for a small UAV.

**Keywords**

UAV, landing gear, aerodynamics, performance, CFD

## 1. ABBREVIATIONS

| | | |
|---|---|---|
| BSFC | = | brake specific fuel consumption |
| $C_D$ | = | drag coefficient |
| $C_L$ | = | lift coefficient |
| $C_P$ | = | power coefficient |
| $C_T$ | = | thrust coefficient |
| HTVT | = | horizontal tail and vertical tail |
| LG | = | landing gear |
| m | = | mass |
| MTOM | = | maximum take-off mass |
| $P_b$ | = | brake power |
| s | = | distance |
| SIMPLE | = | semi implicit method for pressure linked equations |
| RANS | = | Reynolds Averaged Navier Stokes |
| UAV | = | unmanned aerial vehicle |
| ZFM | = | zero fuel mass |
| α | = | angle of attack |
| Δ | = | difference |

## 2. INTRODUCTION

An aircraft's landing gear is a typical component, which is necessary for its operation, however undesirable in terms of aerodynamics. Landing gears produce significant amounts of parasite drag and have a large impact on aircraft weight. Landing gear design has come a long way from simple fixed-gear constructions in pre-World War I aircraft to designs applying fairings and later to retractable landing gears that have revolutionized aircraft performance. They are today an integral part of commercial transport aircraft [1]. Landing gear design has always been considered a challenge as a compromise between ground stability, load requirements and the landing gear's weight and aerodynamic impact has to be found.

While a retractable landing gear greatly decreases parasite drag, it also increases the landing gear's weight and complexity [2]. For large transport aircraft the advantages clearly overweigh. This is different for smaller aircraft where most designs feature fixed gears to avoid the potential complexity and weight penalties [2,3]. This holds true for manned applications as well as small unmanned aircraft (UAVs). Typical UAV landing gears are tricycle designs with the main gear in one part (a spread out fork configuration). Trends indicate that nowadays most UAV landing gears are designed towards simplicity, while aerodynamic shaping is neglected [4].



doi:10.25967/480058

However, with the steadily increasing competition in the unmanned aviation sector, a sophisticated aerodynamic optimization of a new unmanned aircraft becomes crucially important to develop a competitive product. In a recent publication by the authors [5] it was shown that landing gear drag can be as high as 15-28% of a UAV's parasite drag. In such, it is of high interest to investigate, whether an improved landing gear design or even a retraction can significantly enhance flight performance.

This publication shows a performance study for three different UAV landing gear designs. A fixed-unfaired gear, a fixed-faired gear and a retracted gear. The landing gear's weight increase due to retraction or fairings is treated as a variable. This allows to analyze its impact on overall flight performance and indicates a compensation point, where weight increase outweighs aerodynamic improvement.
UAVs are often restricted to a specific maximum take-off mass. Today, civil German regulations prohibit the use of UAVs with maximum take-off masses above 25 kg [6]. On a military basis NATO STANAG 4703 [7] describes simplified airworthiness requirements for UAVs below 150 kg take-off mass. It is critical to stay within such limits or to generally keep the maximum take-off mass (MTOM) constant, if modifications are planned on an existing design. Increasing MTOM might also requires changes to the overall configuration in terms of engine power or safety requirements.
Assuming a constant MTOM and payload, in combination with a reciprocating engine propulsion system, a higher landing gear weight consequently leads to a reduction in fuel capacity. These two effects are mutually reinforcing and might significantly affect range and endurance capabilities. The performance study in this publication includes both investigations of the aerodynamic improvements of different landing gears as well as their weight impact.

Reynolds Averaged Navier Stokes CFD simulations are used to investigate the drag savings of a retracted and a faired landing gear configuration, compared to a fixed-unfaired baseline landing gear. A complete drag break-down is presented for each configuration. The simulated aircraft drag polars are coupled with an incremental flight performance algorithm that allows to simulate typical design mission scenarios. The results are extrapolated to develop a decision workflow that can estimate whether the implementation of a retractable landing gear, the application of fairings or an unfaired landing gear are best suited for other small UAVs.

Following this introduction, chapter 3 describes the methodology including the UAV configuration and the simulation approach, while chapter 4 presents both the results of the numerical simulation and the performance calculation. Chapter 5 gives a comprehensive conclusion.

## 3. METHODOLOGY

### 3.1. UAV configuration

The investigations within this study are performed for a small reconnaissance UAV. Its geometry is created for research purposes. Nevertheless, its configuration is representative for a wide variety of small reconnaissance UAVs [5]. It is a twin tail boom configuration with a rectangular fuselage and high aspect ratio wing. The empennage is configured as an H-tail, attached to tail booms with a circular cross section. An EO/IR payload is located in front of the nose landing gear to enhance visibility. Communication is provided by a wing-like antenna on the fuselage top. The propulsion system is not included in the model. Table 3.1 gives information about the main geometry properties while Fig. 3.1 provides an isometric view.

Table 3.1 Geometry information of generic UAV configuration

| Wing span, m | Aspect-Ratio | Length, m | Ref. area, m² |
|---|---|---|---|
| 3.60 | 9.82 | 2.2 | 1.32 |

Fig. 3.1 Isometric view of generic UAV configuration

The UAV is designed for a maximum take-off mass of 25 kg to stay within the weight limitations according to German official regulations. Its empty mass is estimated by means of an empirical regression analysis for UAVs as proposed by Finger [8] and here shown in Eq. (1).

$$\frac{W_e}{W_0} = 0.699 \cdot {W_0}^{-0.051} \tag{1}$$

This empty mass includes the mass of a typical fixed landing gear. For the following analysis however, it is necessary to extract the landing gear mass from the total empty mass. This allows a later adjustment for the retracted landing gear configuration. Gundlach [9] estimates UAV landing gear weight to be 5% of the maximum take-off mass. This value was proven to be very accurate in the design and construction of another research UAV at FH Aachen and is chosen for the weight estimation in this study.
A representative EO/IR gimbal payload with an assumed mass of 3.5 kg is chosen as the design payload. This configuration is the baseline for the later aerodynamic and performance estimation. A comprehensive mass break-down is provided in Table 3.2.

Table 3.2 Mass break-down of baseline UAV configuration

| Mass break-down | kg |
|---|---|
| Empty mass | 14.83 |
| Landing gear mass (included in empty mass) | 1.25 |
| Payload mass | 3.50 |
| Zero fuel mass | 18.33 |
| Fuel mass | 6.67 |
| Maximum take-off mass | 25.00 |

### 3.2. Landing gear configuration

The UAV model can be equipped with three different landing gear configurations:

1. Unfaired (baseline)
2. Retracted
3. Faired

The baseline configuration employs a circular nose strut with the strut being directly morphed into the streamlined front wheel for reasons of simpler grid generation in the numerical simulation. The main gear strut has a rectangular cross section with rounded corners. The wheels are attached to the strut via cylindrical axles. An image of this baseline configuration is given in Fig. 3.2.

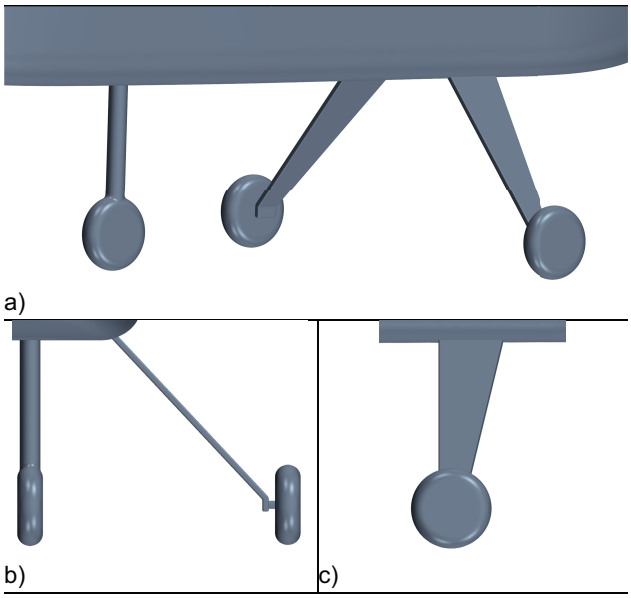


Fig. 3.2 Fixed-unfaired (baseline) landing gear configuration: a) isometric view, b) front view, c) side view of main landing gear

The retracted configuration is simply modelled by eliminating the landing gear from the baseline model and therefore not explicitly shown in an image. Note that no landing gear doors or any kind of gaps due to the retraction mechanism are included in the model.

The faired landing gear configuration is a derivation of the unfaired one, where the main gear struts are replaced with sections of a NACA 0014 airfoil. An image of the faired landing gear configuration is provided in Fig. 3.3.

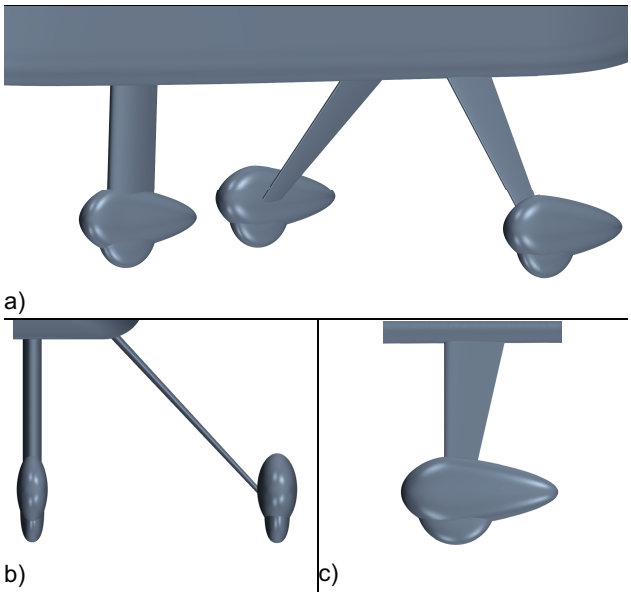


Fig. 3.3 Fixed-faired landing gear configuration a) isometric view, b) front view, c) side view of main landing gear

Care was taken to ensure that the new struts have at least the same thickness as the original ones, to provide comparable structural behavior. The chord length was adjusted according to that. The front gear strut is replaced by a NACA 0030 section and its chord length adjusted as above. All wheels are enclosed by flat droplet shaped fairings. Note that all modifications are not an optimized solution but rather designed with experience and visual aerodynamic considerations.

### 3.3. Simulation approach

The UAV geometry is defined in NASA's OpenVSP [10] and transferred to the commercial simulation software StarCCM+. A steady-state Reynolds Averaged Navier Stokes approach with the SST k-ω (Menter) turbulence model is used to investigate the aerodynamic performance of all three configurations. A more sophisticated description of the RANS approach is beyond the scope of this paper and the reader is kindly referred to Hirsch [11].
The turbulence model is manipulated with a quadratic constitutive relation providing a non-linear relation between the Reynolds stresses and the mean strain rate. This modification addresses the problem of turbulence being simplified as an isotropic process within all classical two-equation turbulence models. More details can be found in the publication by Nagapetyan et al. [12]. A Semi Implicit Method for Pressure Linked Equations (SIMPLE) is applied to solve the incompressible RANS equations with a cell centered finite volume method [13]. The simulations are conducted as freestream simulations with a bullet shaped flow domain

(length: 30 m, width and height: 20 m) with the outline presented in Fig. 3.4 a).

The meshing algorithm of StarCCM+ is used to create a high-quality unstructured mesh consisting of a Cartesian cut cell approach and a dedicated prism layer mesh. The prism layer mesh is only present in the close vicinity of any surface to adequately discretize the boundary layer. The boundary layer thickness is initially estimated for each UAV component individually, with empirical methods presented in Schlichting [14]. The actual thickness is then adjusted within numerous computational iterations to ensure that the total boundary layer of each component is covered by the prism layer mesh. The boundary layer is directly discretized with a low y+ approach consisting of 25 cell layers and a first cell height guaranteeing a y+ < 1 everywhere in the domain. The surface mesh is very fine and adapted to the individual component size with cell edge lengths ranging from 1 mm to 6 mm. A visual impression on the level of mesh refinement is exemplarily provided by a close-up view of the inboard right tire fairing of configuration number 3 (see Fig. 3.4 b). The surface mesh is depicted in white color, while the light blue color shows free volume cells on a surface created for visualization purposes.

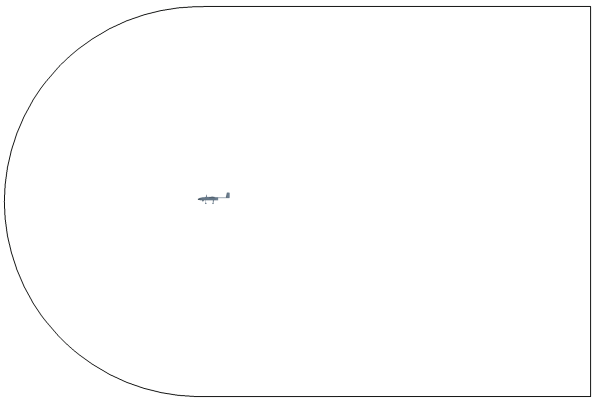

a)

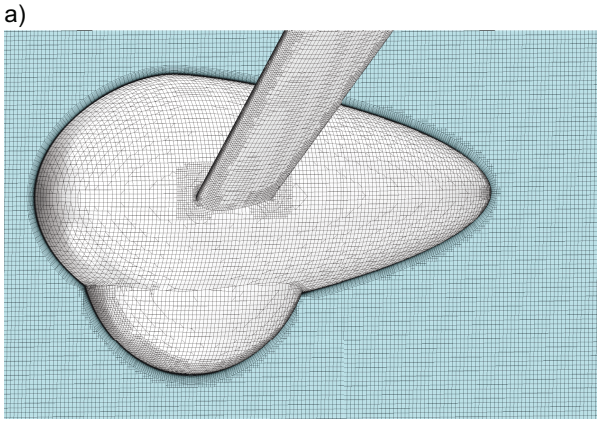

b)

Fig. 3.4 a) domain size, b) local surface mesh on right tire fairing of configuration 3

Lift and drag forces are calculated by multiplying both the local stress tensor and pressure with the cells' face area vector. A summation of all surface cell values around the respective bodies yields to total forces.

An overview about the most relevant simulation parameter is given in Table 3.3.

Table 3.3 Simulation parameter: Mesh, physics, turbulence model

| Simulation parameter | |
|---|---|
| Domain dimensions | 30 m x 20 m x 20 m |
| Surface cell size (depending on component) | 1 mm-6 mm |
| Inlet velocity | 20 m/s |
| Reference pressure | 101325 Pa |
| Density | 1.225 kg/m³ |
| Dynamic viscosity | $1.81205 \times 10^{-5}$ Pa s |
| Turbulence intensity at inlet | 1% |
| Turbulent viscosity ratio at inlet | 10 |

An automated adaptive mesh refinement algorithm provides additional cells in regions with high flow gradients. This creates very effective local refinements and is also applied as a method to perform a grid dependency study. The process is outlined in more detail in the publication by Götten et al. [5] but will be repeated here as a courtesy:
A rather coarse mesh is initially created and a solution run until satisfactory convergence, measured in terms of residual drop and asymptotic integrated values. An algorithm detects areas in which the turbulent kinetic energy exceeds a certain threshold (here set to unity). Within this volume all cell edges are split in half. Coarsening functions are used to slowly blend the mesh from areas of high refinements to areas with larger cells. The simulation is run again with the new mesh refinements in place and the process repeated until grid independent results are observed.
The landing gear shape differs between the unfaired and faired configuration and so do the flow gradients within their wakes. This necessarily leads to different local mesh refinements based on the outcome of the refinement algorithm and requires individual grid dependence studies for each configuration.

The results of a grid dependence investigation based on the total drag coefficient for 5° angle of attack are shown in Fig. 3.5. The unfaired landing gear configuration requires the highest cell count and gives acceptable grid independent results starting with 35 million cells onwards. The faired and retracted configuration indeed require approximately 10 million cells less.

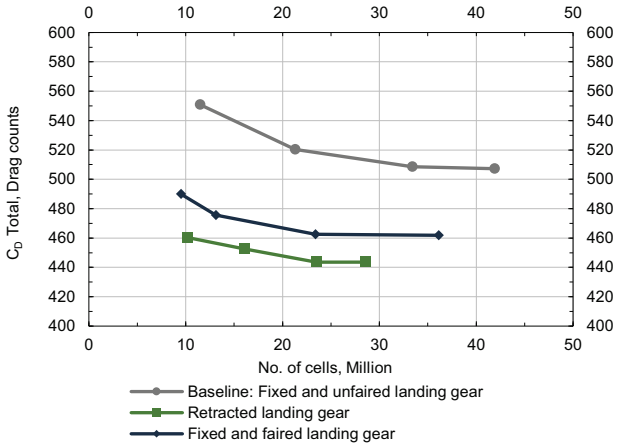


Fig. 3.5 Grid dependence test with automated mesh refinement

The necessity of stronger local mesh refinements is also evident in the volumetric rendering of the Q-criterion (see Fig. 3.6) indicating strong vortical structures in the wake of the unfaired landing gear. The Q-criterion defines a vortex as a connected region with a positive second invariant of the velocity gradient tensor. A vortex is identified in regions where Q>0. [15]
The resolution of strong vortical structures in the unfaired landing gear's wake requires a fine discretization and thus a higher cell count. With fairings applied, the flow behind the landing gear is much more uniform and vortices are restricted to the wake region of the tire fairings. This visualization also implies a significantly higher flow separation for the baseline configuration and indicates higher drag.

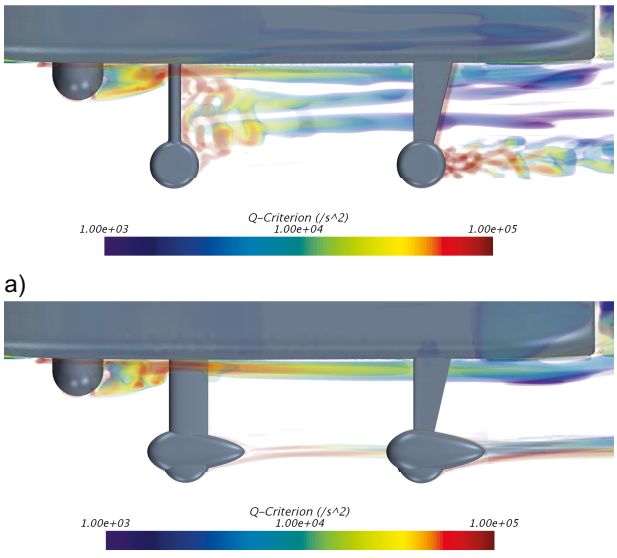


Fig. 3.6 Volumetric rendering: Q-criterion, a) unfaired, b) faired landing gear

### 3.4. Flight performance algorithm

The UAV's flight performance is calculated with an in-house performance code that subdivides a specified mission into multiple sub segments of constant flight distance. A flowchart showing the complete algorithm structure is provided in Fig. 3.7. The algorithm requires a flight mission to be provided as a basic input. This flight mission starts with liftoff and ends with touchdown of the aircraft. Climb, cruise, loiter and descend segments are labelled as such and the algorithm automatically calculates the optimal flight speed for the respective segments based on the aerodynamic input model. Additionally, a defined speed can be provided and the required lift is adjusted according to that. The minimum safely flyable speed is assumed to be 1.2 x $V_{stall}$. In case, an optimum speed is slower than this, the minimum speed is chosen. Besides the flight mission, the aircraft's zero fuel mass and its fuel mass is provided as an input. In the current study the UAV's maximum take-off mass is fixed to 25 kg while both zero-fuel mass and the fuel mass are subject to changes based on the configuration (see in detail paragraph 4.2.1)

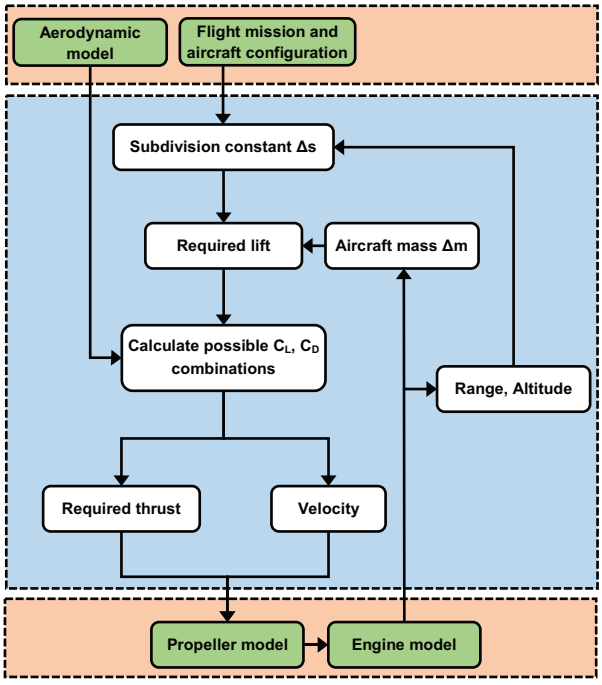


Fig. 3.7 Flight performance algorithm flowchart

An aerodynamic input model is provided in terms of a lift and drag polar. These polars are directly taken from the CFD analysis of the respective UAV configuration. Additionally, an engine model is required to provide power and fuel consumption measures while the accuracy can be enhanced by an optional propeller model. If the propeller model is included, the propeller power and thrust characteristics are specifically included, otherwise a velocity dependent propeller efficiency is assumed. The structure within the

blue region of Fig. 3.7 is the actual incremental flight performance calculation which requires the outside standing models as constant inputs.

The study aims towards the most realistic flight performance calculation as possible, which is why a specific two-stroke engine (3W-55i) and propeller (APC 22x10) were chosen. A detailed analysis of the power characteristics and fuel consumption of the engine is provided by Rowton [16], while propeller data is directly taken from the manufacturer [17]. The engine data used in the performance analysis is shown in Fig. 3.8, propeller data is given in Fig. 3.9. Altitude effects on engine performance are modelled according to Husaboe et al. [18] who provides a modification of the well-known Harari and Sher engine model.

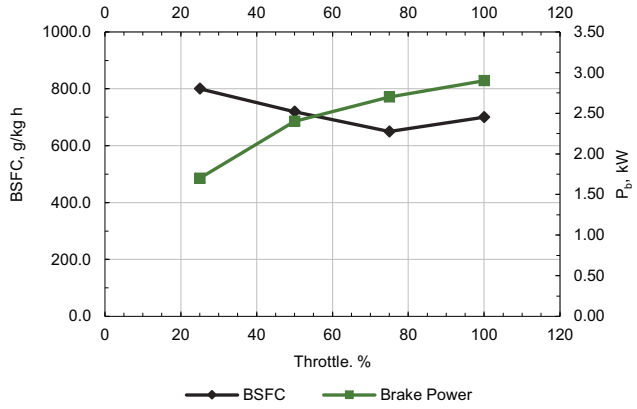


Fig. 3.8 Engine power and fuel consumption, data from [16]

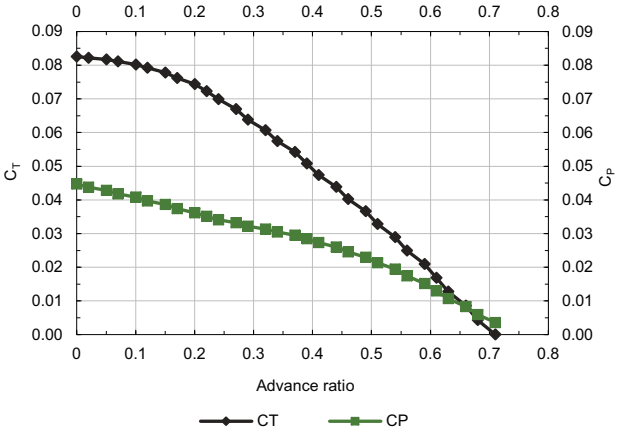


Fig. 3.9 Propeller thrust and power characteristics, data from [17]

## 4. RESULTS

The following section provides the results of the numerical simulation in terms of a drag break-down and complete aircraft polars. The results of this analysis are used as the aerodynamic model input for the flight performance algorithm.

### 4.1. Numerical simulation

The numerical simulations were conducted for angles of attack ranging from -2° up to 15°. The analysis revealed, that the UAV's lift is independent on the landing gear configuration and showed equal $C_L$ vs α curves. The curve valid for all three configurations is shown in Fig. 4.1.

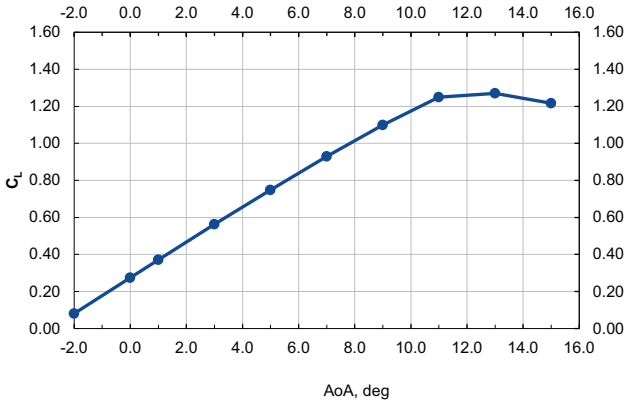


Fig. 4.1 Lift coefficient vs angle of attack

Stall occurred at 13° angle of attack corresponding to a lift coefficient of 1.267. To ensure safe flight with enough margin towards stall speed ($V_{min}$=1.2x$V_{stall}$), the maximum flyable lift coefficient is 0.88. All following diagrams are therefore restricted to a maximum angle of attack of 7° corresponding to a lift coefficient of 0.92. The minimum lift coefficient analyzed is 0.081 and close to a zero-lift condition. Fig. 4.2 shows the drag polar for the fixed-unfaired landing gear configuration. The minimum drag coefficient close to zero lift is 0.03284. Individual polars reveal the contribution of the major aircraft components (wing, empennage, fuselage, landing gear) towards the total drag. The unfaired landing gear contributes to 19% of the total drag close to a zero-lift condition and 12% at the maximum flyable lift coefficient.

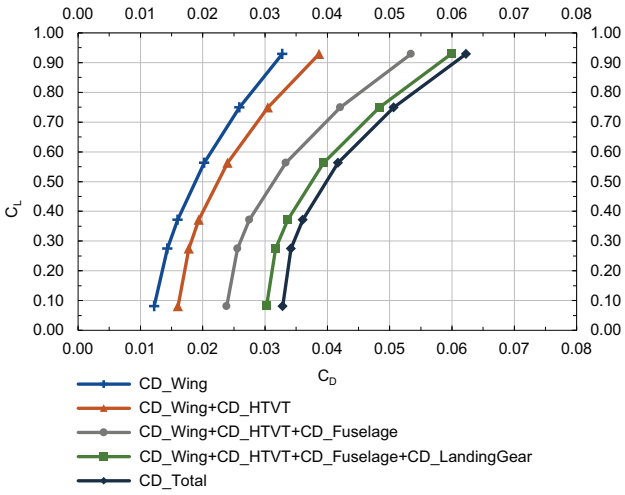


Fig. 4.2 Drag polar and drag break-down, unfaired landing gear

With the landing gear retracted, the drag polar is parallel shifted to the X-axis of the diagram and towards smaller drag coefficients (see Fig. 4.3). Please note that for conformity in this figure, both fuselage and landing gear polar are identical as the landing gear is retracted. The simulation at minimum lift shows a drag coefficient of only 0.02595 and therefore 21% less compared to the fixed-unfaired configuration. This reduction is slightly higher than the percentage drag contribution of the landing gear itself and a reason of omitted interference drag.

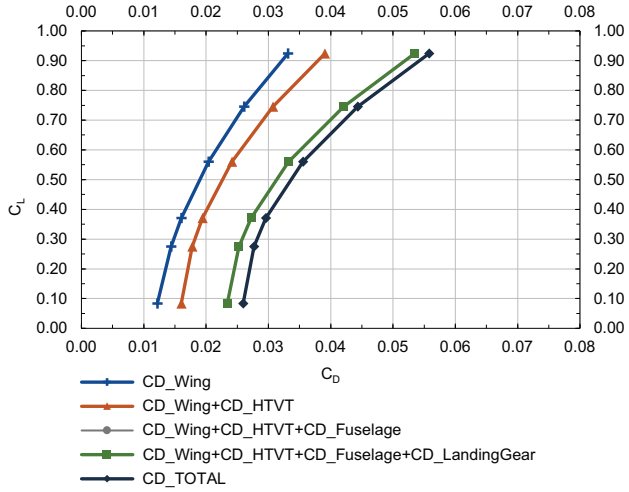


Fig. 4.3 Drag polar and drag break down, retracted landing gear

The effect of fairing the landing gear and optimizing its aerodynamic shape are evident and provided in Fig. 4.4. The minim drag coefficient is now found to be 0.02816 and therefore close to the retracted configuration. Comparing the unfaired and faired configuration a total drag reduction of 14% is found at minimum lift and 9% at maximum flyable lift. The individual drag of the landing gear was reduced by over 70%, proving the new aerodynamic shape to be highly effective.

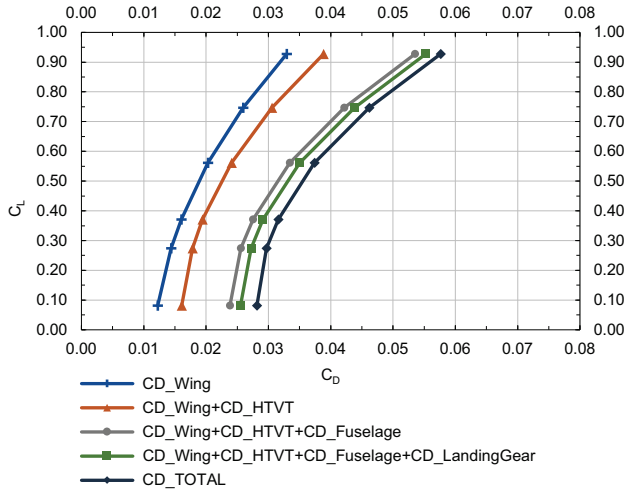


Fig. 4.4 Drag polar and drag break down, faired landing gear

Drag reductions achievable with both the retracted and faired landing gear configuration seem impressive in the first place. However, a closer analysis of the maximum lift-to-drag ratio and power factor reveal that this parasite drag reduction only yields to a small increase in the respective performance factors. Fig. 4.5 and Fig. 4.6 show both the curves of lift-to-drag ratio vs lift coefficient and power factor vs lift coefficient.

A comparison of the aerodynamic performance factors is given in Table 4.1. The retracted landing gear configuration achieves a 10% higher maximum lift-to-drag ratio and power factor, while the faired configuration reaches an 8% gain. Both performance factors are found at high lift coefficients. As landing gear drag stays almost constant with increasing lift, its contribution to the total drag decreases with increasing influence of lift induced drag. For smaller lift coefficients however, the performance gains are significantly higher and a major benefit in this regime can be expected.

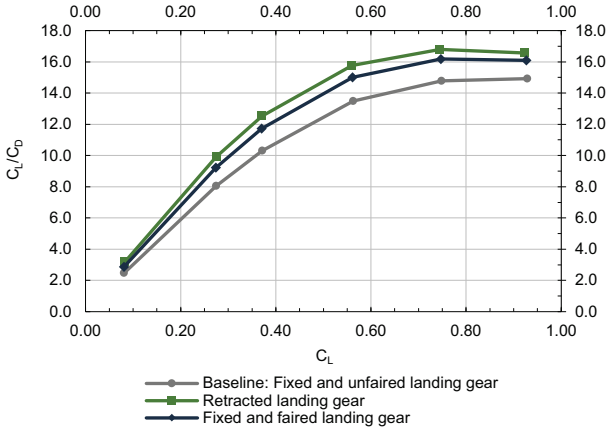


Fig. 4.5 Lift-to-drag ratio comparison

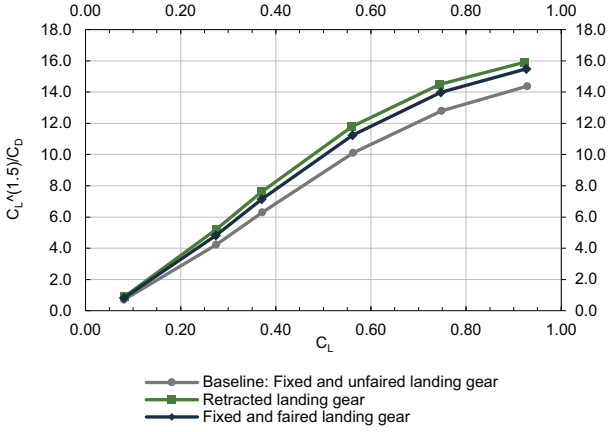


Fig. 4.6 Power factor comparison

Table 4.1 Maximum achievable lift-to-drag ratio and power factor

| | Fixed-unfaired | Retracted | Fixed-faired |
|---|---|---|---|
| $C_L/C_{D\,max}$ | 14.9 | 16.6 (+10%) | 16.1 (+8%) |
| $C_L$^(1.5)/$C_{D\,max}$ | 14.0 | 15.6(+10%) | 15.1(+8%) |
| $C_L/C_D$ at $C_L$=0.3 | 8.0 | 9.9 (+24%) | 9.2 (+15%) |

### 4.2. Flight performance calculation

Most aircraft are designed to a very specific design scenario often termed the “design mission”. However, past experience has shown that during actual operation most aircraft are employed in much more diverse scenarios. This holds true for both manned and unmanned applications [9]. This study accounts for such diverse scenarios by using three different design missions. The performance of each UAV configuration is tested on all three missions, allowing to cover a wide variety of different flight conditions.

#### 4.2.1. Design missions and weight penalty

*1. Long endurance surveillance*

Aim of this mission is to surveil a close by area for as long as possible. A flight altitude of 600 m is chosen as a compromise between communication requirements and camera performance. The UAV performs a circular flight pattern with 2 km radius.

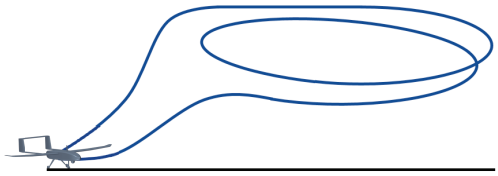

Fig. 4.7 Long endurance mission flight path

*2. Long range reconnaissance*

Within this mission the largest area possible should be covered, which is achieved in the maximum range configuration. Again an altitude of 600 m is chosen.

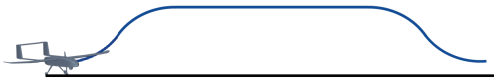

Fig. 4.8 Long range cargo mission flight path

*3. Search and rescue expanding square*

This mission scenario is in accordance to the official aviation search and rescue guidelines of the US Department of Homeland Security [19]. The search starts at the last known location of a missing person or vehicle. The aircraft flies an expanding square pattern for which the leg length is chosen in a way that the camera is able to cover the area below the UAV. To maximize search area, both the flight speed and altitude are optimized under consideration of two constraints:
A point on the ground must be in the camera’s field of view for at least 10 seconds and the minimum image quality must ensure 10 vertical pixels on a standardized human target [20]. Assuming a typical 30x zoom optical daylight sensor with 44° wide field of view and 1.5° tele field of view leads to an optimized altitude of 1380 m and a flight speed of 31 m/s.

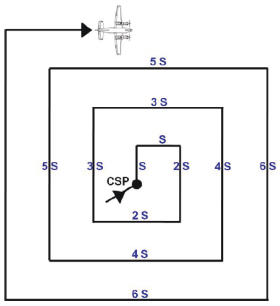


Fig. 4.9 Expanding square SAR flight pattern, taken from [19]

The baseline aircraft configuration features a fixed and unfaired landing gear weighting 1.25 kg (see Table 3.2). The landing gear’s weight increase is handled in terms of a percentage increase compared to the baseline landing gear configuration. Analyses are conducted for weight increases ranging from 5%-85% of the landing gear mass. The combination of UAV zero fuel mass and fuel mass with respect to the landing gear’s weight increase is shown in Fig. 4.10.

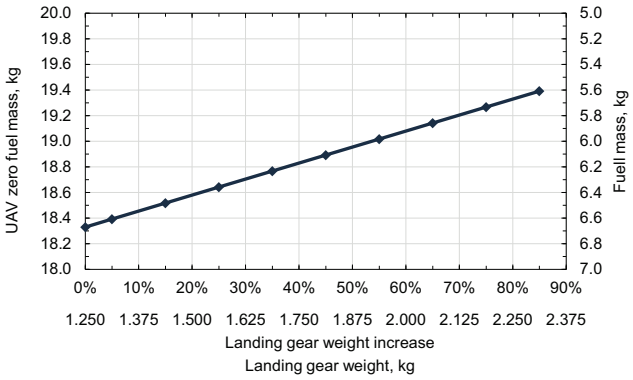


Fig. 4.10 UAV ZFM and fuel mass vs. landing gear weight increase

#### 4.2.2. Design mission performance

*1. Long endurance surveillance*

The analysis revealed a possible flight time of slightly more than 20 hours with the baseline configuration. The impact of retracting or fairing the landing gear are displayed in Fig. 4.11, while Table 4.2 highlights the most important values. The horizontal dashed lines in Fig. 4.11 - Fig. 4.13 indicate the baseline configuration and are only shown for visualization purposes. The analysis assumes a constant landing gear weight of 1.25 kg for the baseline configuration. Both fairing and retracting the landing gear increases the aerodynamic efficiency but lead to an endurance gain only when the weight increase is small. If the retracted landing gear is 37% heavier than the baseline configuration the improved aerodynamic efficiency is completely eradicated by the weight penalty. This compensation point is located at 30% weight increase for the faired landing gear configuration.

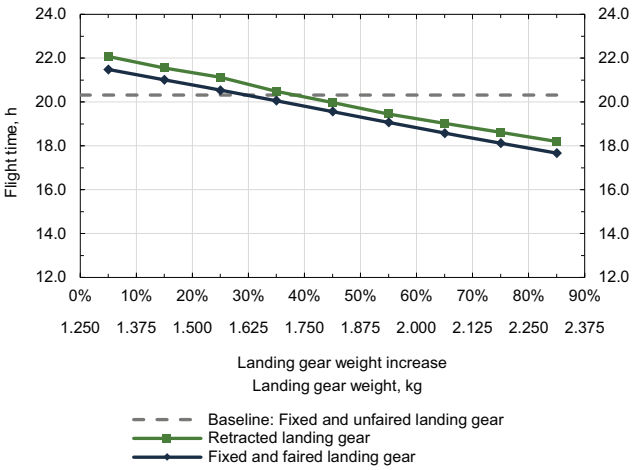


Fig. 4.11 Flight time comparison, mission 1

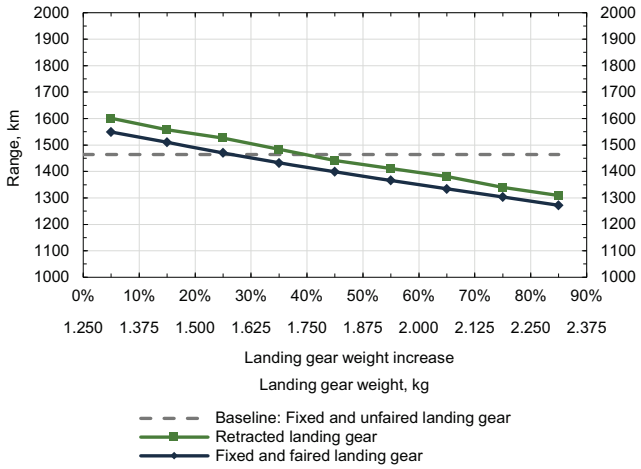


Fig. 4.12 Flight range comparison, mission 2

Table 4.2 Flight performance parameter mission 1

| | Fixed-unfaired | Retracted | Fixed-faired |
|---|---|---|---|
| $C_L$ | 0.88 | 0.88 | 0.88 |
| Speed, m/s | 19.5-17.0 | 19.5-17.1 | 19.5-17.1 |
| Performance gain at 5% LG weight increase | - | 9% | 6% |
| Compensation point in % LG weight increase | - | 37% | 30% |

Table 4.3 Flight performance parameter, mission 2

| | Fixed-unfaired | Retracted | Fixed-faired |
|---|---|---|---|
| $C_L$ | 0.74 | 0.74 | 0.74 |
| Speed, m/s | 20.7-17.7 | 20.7-17.7 | 20.7-17.7 |
| Performance gain at 5% LG weight increase | - | 9% | 5% |
| Compensation point in % LG weight increase | - | 40% | 27% |

Kundu [21] estimates the weight increase of a retractable landing gear compared to a fixed one to be in the order of 15%-25%. Applying this weight increase to the findings of the current study reduces the performance gains below 4%. In such, implementing a retractable landing gear in terms of a long endurance mission gives only a marginal benefit. Such a behavior is typical for small reconnaissance UAVs and the authors believe it is justifiable to extend the following statement beyond the context of this single analysis: If maximum take-off mass is limited as a constraint, the implementation of a retracted landing gear is not beneficial for small reconnaissance UAVs on long endurance missions. Fairing the landing gear might only lead to a slight weight impact if proper design techniques are used. Assuming a weight increase of 5% the endurance is extended by 6% which is able to outperform the retracted configuration.

*2. Long range reconnaissance*

The UAV's maximum range is 1460 km without any reserve in the baseline configuration. Comparable to the long endurance mission the performance gains by retracting or fairing the landing gear are rather small (see Fig. 4.12 and Table 4.3). The compensation point is located at 40% weight increase for the retracted configuration and 28% for the faired configuration. Again, a performance gain is much more realistic with a faired landing gear, while the general impact is limited to about 5% range increase for a 5% heavier landing gear.

*3. Search and rescue expanding square*

This mission scenario is very different from the previously described ones as a fixed speed of 31 m/s is used. This reduces the lift coefficient in flight to around 0.3 and thus far away from the optimal lift-to-drag ratio. As presented in Table 4.1, the aerodynamic efficiency gain is much higher at low lift coefficients and thus are performance gains in the mission analysis (see Fig. 4.13 and Table 4.4). The compensation points are shifted to 55% landing gear weight increase for faired and 75% for retracted configuration.

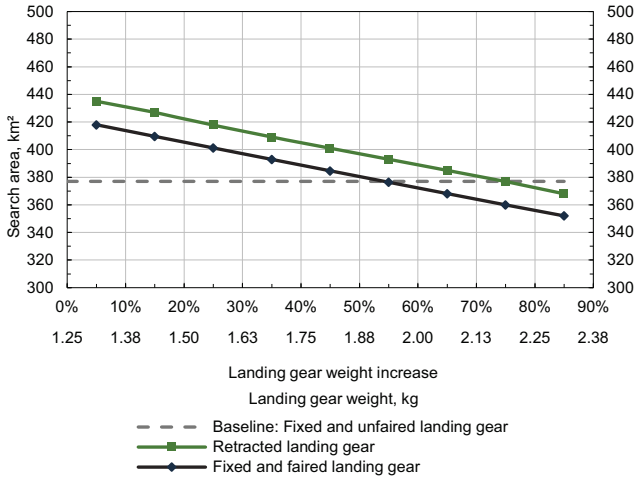


Fig. 4.13 Search area comparison, mission 3

Table 4.4 Flight performance parameter, mission 3

| | Fixed-unfaired | Retracted | Fixed-faired |
|---|---|---|---|
| $C_L$ | 0.26-0.36 | 0.26-0.36 | 0.26-0.36 |
| Speed, m/s | 31 | 31 | 31 |
| Performance gain at 5% LG weight increase | - | 15% | 11% |
| Compensation point, in % LG weight increase | - | 75% | 55% |

With an estimated landing gear weight increase due to the retraction mechanism of 25% (see above and [21]), a 10% higher search area is achieved. It is likely that the weight increase due to fairings is much less compared to a retraction mechanism. To achieve the same performance gains as with the retracted landing gear, the weight increase due to fairings must not be higher than 10% of the landing gear's mass. In such a case, the faired configuration is preferable due to its simplicity.

### 4.2.3. Landing gear design decision criterion

The present analysis only describes one UAV configuration and other configurations might lead to slightly different behavior. Götten et al. [5] showed that multiple twin-tail boom UAVs between 30 kg and 500 kg have very comparable parasite drag behavior. The authors believe that such aerodynamic similarities allow to extrapolate the findings of this study to other UAVs of the above category. In such, the present analysis is suited for developing a universal landing gear decision criteria for this UAV class, shown in Fig. 4.14.

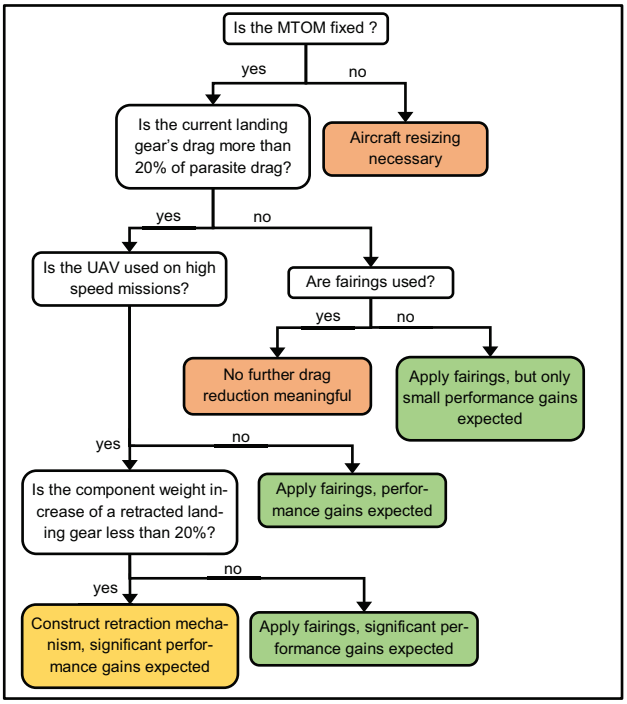


Fig. 4.14 Landing gear design decision flowchart

This decision workflow shows that the application of a retracted landing gear in the above described UAV class is only reasonable for pure high speed mission scenarios. Furthermore, significant performance gains might only be achieved if the weight increase is kept in the order of 20% of the fixed gear weight. In all other cases designing a well faired fixed landing gear outperforms the weight penalties of the retraction mechanism.

## 5. CONCLUSION

The present analysis has shown both the aerodynamic and flight performance impact of exchanging a fixed and unfaired landing gear with a retracted gear or a well faired one for a small reconnaissance UAV. Retracting the landing gear reduced parasite drag by more than 20%. The application of fairings was shown to be very effective and lead a total parasite drag reduction of 14%. This coincides with a reduction of landing gear drag by over 70%. The aerodynamic performance differences between a well faired UAV landing gear and a retracted one were shown to be comparably low.

As landing gear drag is nearly constant with respect to the aircraft's lift coefficient, its influence on the lift-to-drag ratio reduces at higher lift coefficients. A performance analysis revealed that using a retracted or a faired landing gear on UAV-typical low speed missions yields only to very small performance enhancements. Even without any weight penalties, the gains were shown to be no more than 10%. Considering the inevitable weight increase of a retracted landing gear, the aerodynamic efficiency increase is quickly eaten-up by the added weight. Applying fairings, might only slightly increase the landing gear's weight and can therefore outperform a retracted landing gear configuration. Performance gains are still restricted to values in the order of 5%. Retracting a landing gear comes at a much higher price concerning weight penalties, complexity and safety requirements.
Missions with high speed flights might benefit significantly more from both a retraction and fairing of a UAV's landing gear. An exemplary design mission revealed performance gains above 15%. This is however only the case if the weight penalty is assumed to be small. With increasing landing gear weight the performance gains quickly reduce. Again it was shown that a faired solution is well able to outperform a retracted configuration just by a reduction in component weight.

Due to aerodynamic similarities of twin-tail boom UAVs the findings of this study might be extrapolated to similar UAVs up to 500 kg MTOM.
A new decision workflow is presented which allows designers to quickly analyze if fairing or retracting a UAV's landing gear is adequate. In most cases the application of fairings is more meaningful.

**REFERENCES**


[1] Anderson Jr., J. D., *The Airplane*, American Institute of Aeronautics and Astronautics, Inc, Reston, VA, 2003.

[2] Stinton, D., *The design of the aeroplane*, Blackwell Science, Oxford, 1995.

[3] Austin, R., *Unmanned aircraft systems. UAVS design, development and deployment,* 2nd edn., Wiley, Chichester, Hoboken, 2010.

[4] Shephard, *Unammed Vehicles Handbook 2008*, The Shephard Press Ltd, Berkshire, UK, 2008.

[5] Götten, F., Havermann, M., Braun, C., Gómez, F., and Bil, C., "On the Applicability of Empirical Drag Estimation Methods for Unmanned Air Vehicle Design," *18th AIAA Aviation Technology Integration and Operations Conference,* American Institute of Aeronautics and Astronautics, Reston ,VA, 2018.

[6] Bundesministerium für Verkehr und digitale Infrastruktur, *Verordnung zur Regelung des Betriebs von unbemannten Fluggeräten. Drohnenverordnung*.

[7] NATO, "Light Unmanned Systems Airworthiness Requirements," NATO Standardization Office, Brussels, 24.11.2016, No. 4703.

[8] Finger, D. F., "Comparative Performance and Benefit Assessment of VTOL- and CTOL-UAVs," *Deutscher Luft- und Raumfahrtkongress 2016*.

[9] Gundlach, J., *Designing Unmanned Aircraft Systems: A Comprehensive Approach,* 2nd edn., AIAA Education Series, Washington, DC, 2014.

[10] Gloudemans, J., Davis, P., and Gelhausen, P., "A rapid geometry modeler for conceptual aircraft," *34th Aerospace Sciences Meeting and Exhibit,* American Institute of Aeronautics and Astronautics, Reston, Virigina, 1996.

[11] Hirsch, C., *Computational methods for inviscid and viscous flows*, Wiley, Chichester, 2002.

[12] Nagapetyan, H., Wray, T., and Agarwal, R., "Application of the Quadratic Constitutive Relation to Various Turbulence Models in OpenFOAM," *46th AIAA Fluid Dynamics Conference,* American Institute of Aeronautics and Astronautics, Reston ,VA, 2016.

[13] Ferziger, J. H., and Perić, M., *Computational Methods for Fluid Dynamics*, Springer, Berlin, Heidelberg, s.l., 2002.

[14] Schlichting, H., and Gersten, K., *Boundary-Layer Theory,* 9th edn., Springer Berlin Heidelberg, Berlin, Heidelberg, s.l., 2017.

[15] HALLER, G., "An objective definition of a vortex," *Journal of Fluid Mechanics*; Vol. 525, 1999, pp. 1–26. doi: 10.1017/S0022112004002526.

[16] Rowton, A. K., *Measuring scaling effects in small two-stroke internal combustion engines*, Wright Patterson Air Force Base, Ohio, 2014.

[17] APC Propeller, "Propeller Measurement Data 22x10," https://www.apcprop.com/files/PER3_22x10.dat, [retrieved 21 June 2018].

[18] Husaboe, T. D., Polanka, M. D., Rittenhouse, J. A., Litke, P. J., and Hoke, J. L., "Dependence of Small Internal Combustion Engine's Performance on Altitude," *Journal of Propulsion and Power*; Vol. 30, No. 5, 2014, pp. 1328–1333. doi: 10.2514/1.B35133.

[19] Department of Homeland Security, "Land Search and Rescue Addendum: National Search and Rescue Supplement to the International Aeronautical and Maritime Search and Rescue Manual," 2011, http://www.mngeo.state.mn.us/committee/emprep/download/USNG/2011_1118_Published_Land_SAR_Addendum_1.0.pdf, [retrieved 11 July 2018].

[20] Lumang, M. A., "Long-Range Surveillance Cameras & Johnson's Criteria: White-Paper on Long-Range Surveillance Cameras," http://www.aissecuritysolutions.com/white-paper-on-long-range-surveillance-cameras.pdf, [retrieved 11 July 2018].

[21] Kundu, A. K., *Aircraft design*, Cambridge University Press, Cambridge, 2010.